

Transferrable SERS Barcodes

Furkan Sahin, Sami Pekdemir, Menekse Sakir, Zehra Gozutok, and Mustafa Serdar Onses*

The demand for encoded surfaces has increased significantly over the past decade driven by the rapid digitalization of the world. Surface-enhanced Raman scattering (SERS) offers unique capabilities in generation of encoded surfaces. The challenge is the limited versatility of SERS-based encoding systems in terms of the applicable surfaces. This study addresses this challenge by using a temporary tattoo approach together with simplified fabrication of SERS-active patterns by ink-jet printing of a particle-free reactive silver ink. Plasmonic silver nanostructures form on the tattoo paper upon ink-jet printing and a brief thermal annealing. The SERS activity is sufficient to detect taggant molecules of rhodamine 6G, methylene blue, and rhodamine B with a nanomolar level sensitivity. Raman-active taggants can be incorporated into the ink, for drop-on-demand patterning of multiple molecules in 1D and 2D barcode geometries. The SERS barcodes can be effectively transferred to a range of different substrates retaining high plasmonic activity and geometric integrity. The presented approach decouples the SERS-active pattern preparation from the final substrate and greatly improves the versatility of the barcodes.

involves counterfeit and pirated goods.^[1] Expectations suggest further increase of such illegal trade considering the ease of access to technologies provided by the internet.^[2,3] Counterfeiting activities not only cause significant loss of income for original product owners, but also threaten human health, adversely affect the economies of countries, and disrupt the social balance.^[4–8] A conventional approach to solving this problem has been the use of security labels.^[9,10] Different forms of barcodes have been developed to encode information. The unique and size-dependent properties of nanomaterials offer unprecedented routes to increase the complexity of such barcodes.^[11,12] Photoluminescent quantum dots,^[13,14] magnetically responsive structures,^[15–17] and plasmonic nanomaterials^[18,19] have been actively used as encoding materials.

The field of plasmonics exploits light-matter interactions in materials that are

confined at the nanoscale. The ability to tune the absorption, fluorescence and scattering of light via plasmonic structures provide novel routes for preparation of encoded surfaces. The focusing of light near plasmonic structures results in strong electric field enhancements. One consequence of such enhancement is amplification of Raman scattering associated from molecules. Commonly referred as surface-enhanced Raman scattering (SERS), this approach has attracted growing interest in applications that range from molecular biology to sensing technologies.^[20–29] SERS provides unique capabilities in anti-counterfeiting applications. First, fingerprint vibrations of molecules observed in Raman spectroscopy enable generation of unique security labels with high levels of encoding capacity. Second, patterning plasmonic structures allow for geometric encoding of information and preparation of different forms of barcodes. Third, the dependence of SERS on the concentration of molecules, polarization of light and other intrinsic characteristics enable formation of additional security layers, further challenging counterfeiters. Several recent efforts have focused on preparation of SERS based barcodes.^[30–42] Ling and coworkers demonstrated the potential of multiplex SERS security labels encoded with multiple probe molecules using spatially and spectrally defined silver plasmonic nanostructures.^[43] Li et al. reported patterning of colloidal silver nanocubes through a stencil mask as flexible SERS barcodes.^[44] In another study, Pekdemir et al. demonstrated microscopic linear SERS-barcodes fabricated by microfluidics assisted fabrication.^[45] In a recent study, SERS inks composed of star-shaped gold nanoparticles and taggants were written with a ballpoint pen for anti-counterfeiting.^[39] Another study showed that Au@SiO₂

1. Introduction

According to a recent report by the Organization for Economic Co-operation and Development and the European Union's Intellectual Property Office, >3% of the global trade

F. Sahin, S. Pekdemir, M. Sakir, Z. Gozutok, M. S. Onses
ERNAM – Erciyes University Nanotechnology
Application and Research Center
Kayseri 38039, Turkey
E-mail: onses@erciyes.edu.tr

S. Pekdemir
Department of Aeronautical Engineering
Faculty of Aeronautics and Astronautics
Erciyes University
Kayseri 38039, Turkey

Z. Gozutok
Department of Textile Engineering
Erciyes University
Kayseri 38039, Turkey

M. S. Onses
Department of Materials Science and Engineering
Erciyes University
Kayseri 38039, Turkey

M. S. Onses
UNAM–Institute of Materials Science and Nanotechnology
Bilkent University
Ankara 06800, Turkey

 The ORCID identification number(s) for the author(s) of this article can be found under <https://doi.org/10.1002/admi.202200048>.

DOI: 10.1002/admi.202200048

core-shell nanoparticle-electrospun fiber composites modified with Raman active molecule can be used to encode QR codes.^[40] All these studies highlight that SERS based encoding is an effective route for anti-counterfeiting applications. The challenge is to develop practical ways for preparing multiplex SERS barcodes and, in particular, overcome the limitations in the applicable substrates.

To address these challenges, we developed a practical, entirely solution-processing based and substrate independent approach for preparation of SERS barcodes. First, we study ink-jet printing of particle-free silver inks to generate SERS-active barcodes. Upon printing and brief heating, the silver inks form plasmonic structures with high-levels of SERS activity. The particle-free ink formulation allows for smooth printing process for additive fabrication of SERS-active patterns. Raman active taggant molecules can be further incorporated in the ink, for one step fabrication of multiplex SERS barcodes, in an analogy to the color printing on a paper. To completely decouple the substrate from the barcode preparation process, we use a temporary tattoo approach. Ink-jet printing of particle-free silver inks on a temporary tattoo paper enables versatile transfer of the SERS barcodes on surfaces of interest. This capability greatly improves the application potential, providing a route for direct attachment of SERS barcodes on goods.

2. Results and Discussion

A schematic representation of our approach to fabricating transferable SERS barcodes is given in **Figure 1**. First, desired patterns, such as barcodes and butterflies, were generated in a computer-aided design program. The colors in the design represent Raman-active taggant molecules. For example, R6G refers to red and MB refers to blue in the design. The particle-free reactive silver ink and its mixtures with Raman-active taggants were added to the cartridges. The printing was carried out on the tattoo paper. Ink-jet printing allows material efficient deposition of inks using low volumes of liquid, thereby enabling deposition of silver patterns without degrading the water-soluble layer of the tattoo paper. In the last step, the printed-tattoo paper was heated at 135 °C for 2 min. This annealing step ensures the reduction of the reactive silver ink and removal of volatile compounds, resulting in the formation of plasmonic silver nanostructures in the printed regions. Plasmonic nanostructures provide enhancement of Raman scattering and thereby SERS activity. The SERS barcodes can now be easily transferred to objects of varying composition, planarity, and stiffness. The tattoo paper is stucked to the object of interest by gentle application of pressure and the backing paper is removed by wiping the surface with a damped cloth (**Figure 1b**). A practical demonstration is shown through the famous the Tortoise Trainer painting. This example demonstrates SERS barcodes can be attached to different goods for anti-counterfeiting purposes (**Figure 1c**). **Figure S1** (Supporting Information) presents a range of different geometries of silver patterns that were attached to a variety of objects and materials, including fruits, vegetables, bone, eggs, fabric, ceramic, wood, glass, and porcelain. The authentication of the SERS-active security labels by Raman mapping is presented in **Figure 1d**.

We first studied the patterning process by ink-jet printing of the particle-free reactive silver ink in the absence of taggant molecules. **Figure 2** presents a structural analysis of the silver inks printed on the tattoo paper. Temporary tattoo papers usually consist of a durable backing paper and a silicon release coating that separates the print from the backing paper. There is also a cellulose-derived transparent transfer layer on the tattoo paper, where the patterns are printed.^[46–48] Upon the printing and thermal annealing process, silver nanoparticles with an average diameter of 152 nm formed on the tattoo paper (See **Figure S2**, Supporting Information for particle size histogram). We hypothesize that the reactive silver ink penetrated throughout the transfer layer, thereby enabling the presence of plasmonic hot-spots on the opposite side, which becomes the air interface following the transfer process. We used XPS analysis to investigate this hypothesis because XPS probes the top surface composition with limited depth of penetration (<5–10 nm). **Figure 2b** presents XPS survey scans of the silver ink printed tattoo paper, before and after the transfer of this sample to the silicon substrate. The XPS measurements showed the presence of Ag, C, O, N, and Si elements on both surfaces. The characteristic peaks associated with C and O are probably due to the cellulose-derived transfer layer, whereas Si element is due to the release layer. As shown in **Figure 2c**, the binding energies of Ag3d peaks at 375.1 and 369.1 eV are attributed to Ag 3d_{5/2} and Ag 3d_{3/2}, respectively. The spin orbital separation of 6 eV confirms the presence of metallic silver (Ag⁰) on both surfaces.^[49] The XRD analysis was performed to examine the crystal structure of these metallic silver nanostructures (**Figure 2d**). XRD peaks located at 38°, 44°, 65°, 77°, and 82° refer to (111), (200), (220), (311), and (222) planes of face-centered cubic crystal structure of metallic Ag (JCPDS, file no. 04-0783), respectively.^[50] Furthermore, the presence of silver on the transferred tattoo was also confirmed by EDX mapping (**Figure S3**, Supporting Information) and EDX elemental analysis. In **Figure 2e**, the EDX spectrum showed a strong peak at ≈3 keV, which correlated with silver and the surface contained 55% silver by weight.

The SERS performance of the fabricated barcodes was studied by analyzing the limit of detection, intensity-concentration relation, and enhancement factor. Varied concentrations of R6G solutions were drop-cast on the barcodes that were transferred to silicon substrates. The characteristic vibrational bands of R6G at positions of 614 cm⁻¹, 773 cm⁻¹, 1364/1649 cm⁻¹ are clearly detected, which are attributed to in-plane C–C–C, out-of-plane C–H, and aromatic C–C stretch vibrational mode, respectively.^[51,52] The Raman spectra of the tattoo paper transferred without the printed silver ink and printed ink in the absence of taggant molecules did not exhibit these characteristic vibrational bands (**Figure S4**, Supporting Information). The characteristic bands of R6G could be detected at concentrations as small as 1 × 10⁻⁹ M (**Figure 3a**). This limit of detection shows that the platform offers a high level of SERS activity. An important figure of merit for SERS platforms is the intensity-concentration relationship (**Figure 3b**). The intensity of the Raman band at 1649 cm⁻¹ scales well with the concentration of the probe molecule. The dependence of the Raman intensity on the logarithm of the concentration can be well represented using a line with a correlation coefficient (*R*²) of 0.983. These

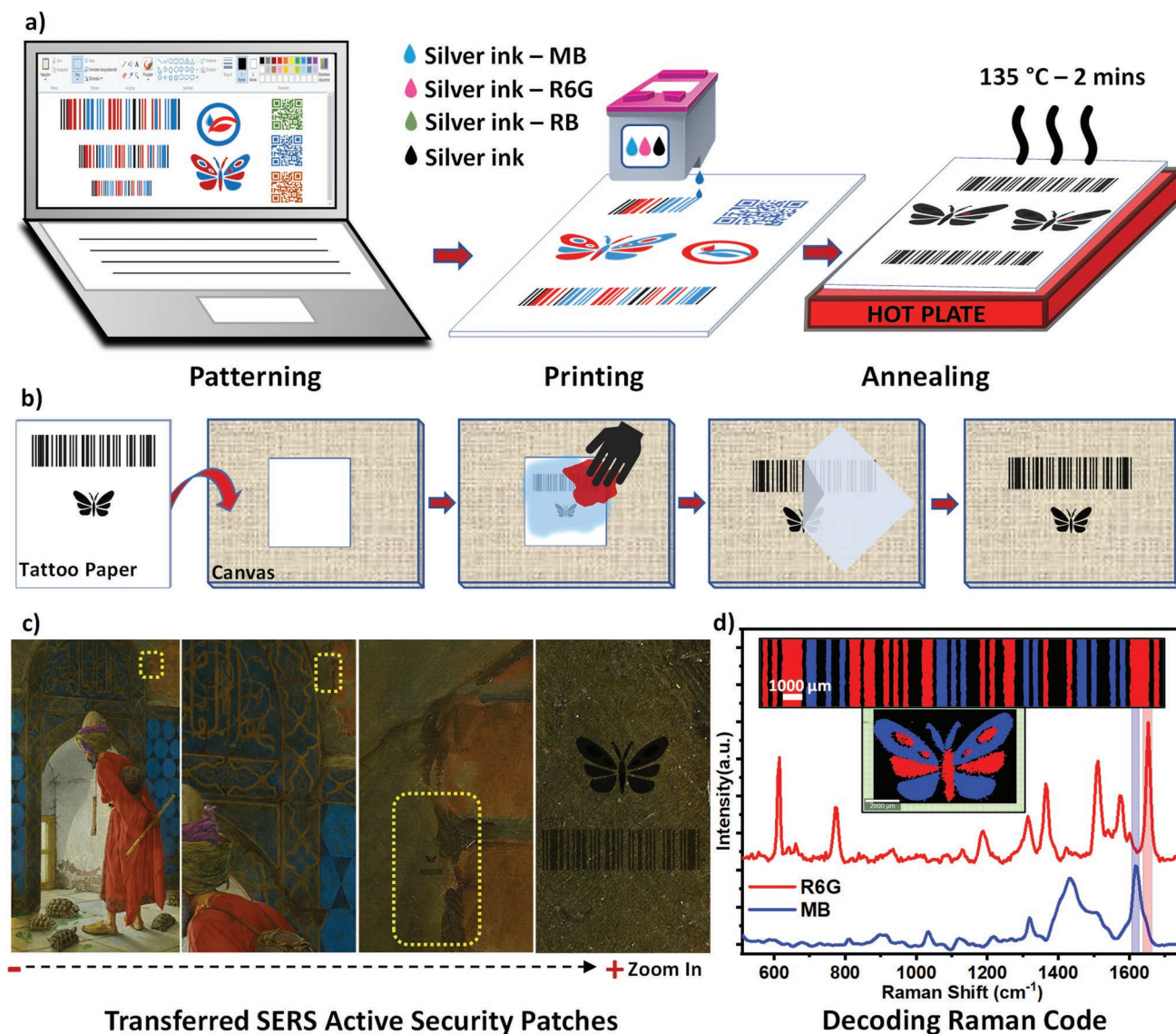


Figure 1. A schematic illustration of the approach for generating transferrable SERS barcodes a) Patterning of SERS barcodes via ink-jet printing on the tattoo paper. Different combinations of particle-free silver and Raman-active taggants are used as inks. b) The process of transferring SERS barcodes. c) A demonstration using a copy of the famous The Tortoise Trainer (Osman Hamdi Bey, oil on canvas, 221,5 × 120 cm. 1906) is found in Suna and İnan Kırac Foundation Orientalist Paintings Collection. The painting was published with permission from Suna and İnan Kırac Foundation. d) Raman spectra and Raman mapping images of the barcodes and butterfly. The Raman mapping images were generated by using the characteristic Raman shifts at 1649 cm⁻¹ and 1624 cm⁻¹ for R6G and MB, respectively.

results support the quantitative determination ability of molecules with the presented transferrable SERS active platform. The SERS performance of the barcodes on the tattoo paper was higher in comparison with the barcodes that were transferred to the silicon substrate (Figure S5, Supporting Information). On the tattoo paper, for example, R6G could be detected at concentrations as small as 10×10^{-12} M, whereas the detection limit was 1×10^{-9} M on the barcodes that were transfer printed. This result shows the high performance of the SERS platform that can be simply fabricated by ink-jet printing of the particle-free silver ink and thermal annealing. The contrast in the SERS performance before and after the transfer process is reasonable considering the structural difference (Figure 2a SEM images) on the top surface of the barcodes. Note that the surface was

brought upside down during the transfer step and the SERS measurements were performed on the two opposite surfaces for the samples before and after the transfer.

The analytical enhancement factor (AEF) was calculated using the equation (1) to measure the SERS performance of the surface. Where $I_{\text{SERS}}(650)$ and $I_{\text{Raman}}(54)$ are the peak intensities at 1649 cm⁻¹ in the spectrum obtained on the SERS barcode and reference Si wafer, respectively. $C_{\text{SERS}}(1 \times 10^{-9}$ M) and $C_{\text{Raman}}(1$ mM) are the concentrations of R6G deposited on these substrates, respectively (Figure S6, Supporting Information). Accordingly, AEF was calculated as 1.2×10^7 . Overall, the SERS characteristics of the presented platform are comparable with recently reported rigid platforms.^[53–58] The SERS activity of the transfer printed barcodes can be attributed to

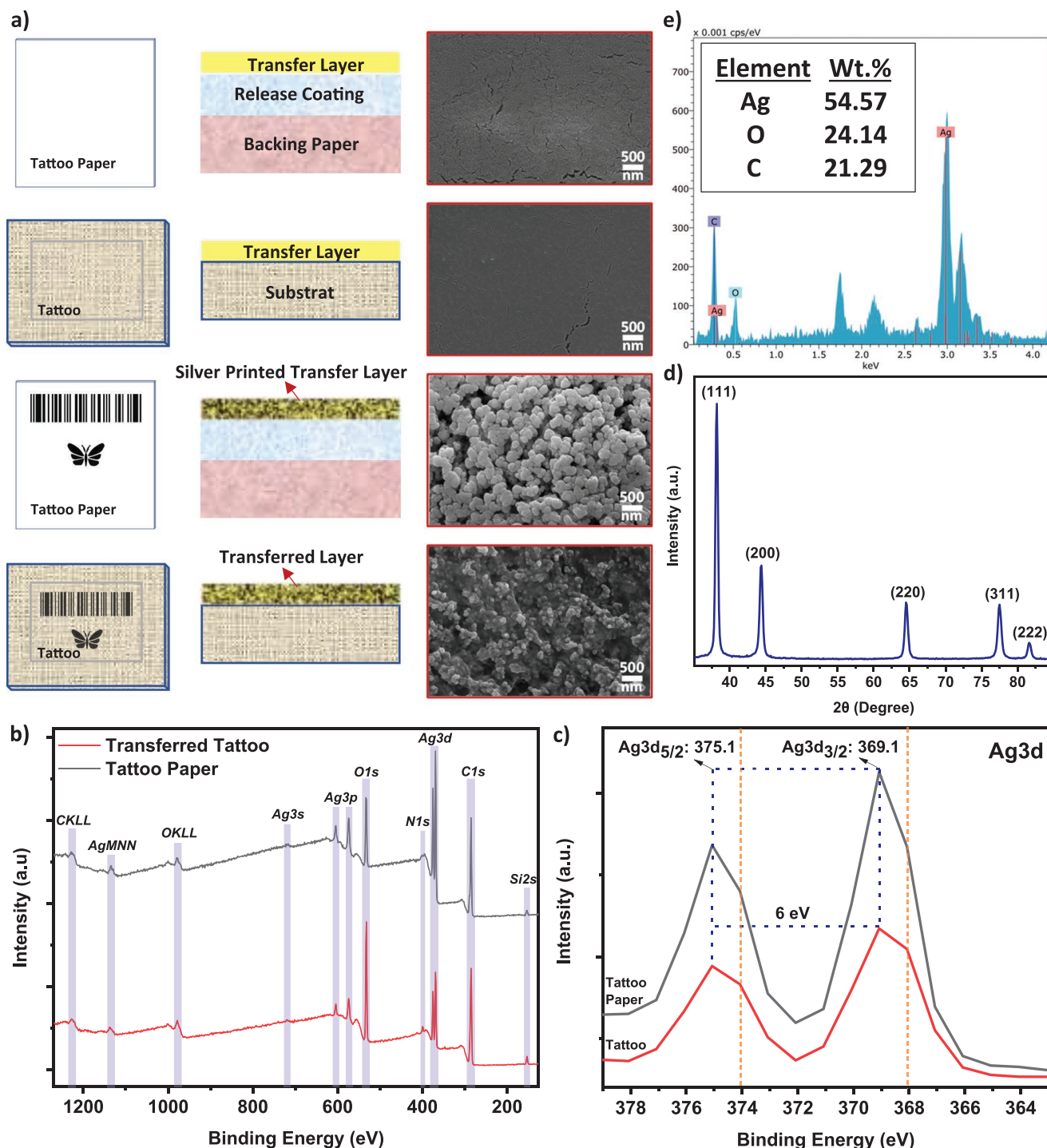


Figure 2. Chemical and structural analysis of SERS barcodes. a) Schematic representation of the tattoo paper structure, printing and transfer process, and corresponding SEM images. b,c) XPS analysis of the silver printed tattoo paper and following the transfer of this sample on the silicon substrate. c) High-resolution regional XPS spectra of Ag 3d. d) XRD diffraction pattern of the SERS barcode. e) EDX elemental analysis of the SERS barcode.

the electromagnetic enhancement mechanism. The formation of silver nanoparticles with small separation distances likely favor formation of plasmonic hot-spots, where strong electromagnetic fields are present. This argument is further supported by the decrease in SERS activity with the increasing number of printed layers (Figure S7a, Supporting Information).

At repeated printing of the ink over the same region the silver particles merge (Figure S7b, Supporting Information) and form a continuous network, which likely reduces the ability to generate plasmonic hot-spots.

The uniformity, reproducibility, and stability of the SERS response are highly important. Figure 3c shows R6G (100 μM)

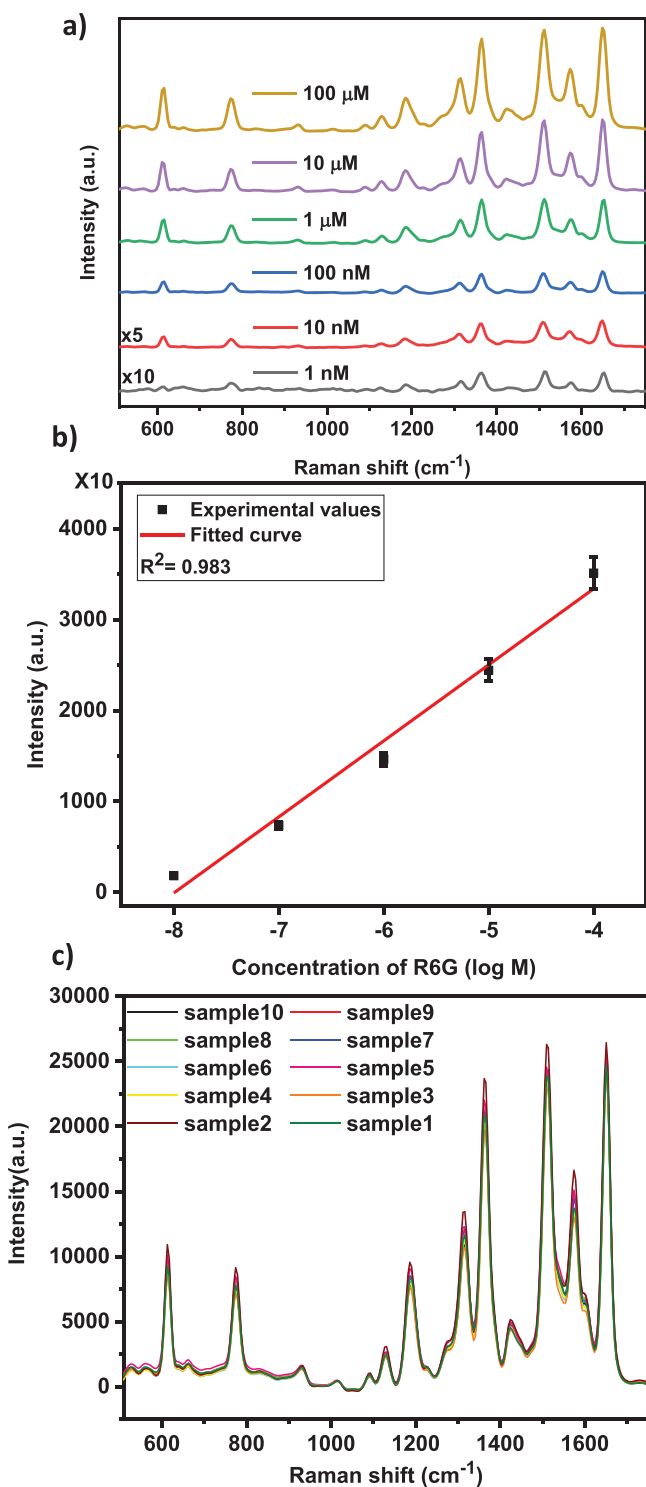


Figure 3. SERS performance characterization. a) Raman spectra of different concentrations of R6G on the SERS barcodes. b) The intensity of the Raman band at 1649 cm^{-1} for varying concentrations of R6G. c) Raman signals collected on ten different samples showing the sample-to-sample reproducibility.

signals collected from ten different SERS barcodes. Signals of approximately the same intensities were collected from all samples. Table S1 (Supporting Information) shows the standard

deviation of the intensities of the R6G characteristic peaks. The percentage of standard deviation to mean is below 8% for all characteristic peaks of R6G, clearly demonstrating the sample-to-sample reproducibility of this SERS response. Similarly, the SERS spectra taken from ten different points across a single substrate were highly uniform (Figure S8, Supporting Information). This uniformity is particularly important in generating Raman mapping images of the barcodes presented later (vide infra). Finally, we investigated the ambient air and mechanical stability of the fabricated SERS barcodes. In a first experiment, the SERS activity of the transferred barcodes was measured after varying periods (15, 30, 45, 60, 90 days) of ambient air storage at dark. Figure S9 (Supporting information) shows that the silver patches retained their activity even after 90 days of ambient storage. The SERS activity showed $\approx 25\%$ reduction after 90 days of ambient air storage in comparison to the freshly prepared samples. This slight decay is likely a result of the oxidation of silver. In another experiment, the freshly prepared SERS barcodes were exposed to sand abrasion for 1 min and then washed with water. The barcodes remained on the surface and the SERS intensity was mostly retained following the sand abrasion (Figure S10, Supporting information). The penetration of the silver nanoparticles to the transfer layer during thermal annealing likely contributes to the adhesion of the barcodes. Collectively, these results support the strong promise of the presented platform for real-world applications.

For effective and practical fabrication of SERS barcodes, it is necessary to simultaneously print taggant molecules and the particle-free silver ink. One particular disadvantage of the subsequent deposition of the taggant molecules on the printed barcodes is the contamination of the entire substrate (Figure S11, Supporting Information). To address this issue and enable one-step fabrication of the SERS barcodes, we investigated direct printing of mixtures of taggant molecules and particle-free silver ink. Figure 4a presents SEM images together with EDX mapping of silver on the barcodes fabricated by printing the mixture of the silver ink and taggants consisting of R6G, MB and RB. Upon the printing and thermal annealing, silver nanoparticles were formed effectively with an average particle size of less than 200 nm (Figure S12, Supporting Information). EDX mapping confirmed the uniform deposition of silver over the substrate. Figure 4b presents XPS analysis of the barcodes fabricated by printing the mixture of particle-free silver inks and taggant. For all three-silver ink-taggant mixtures, the XPS analysis revealed similar composition with characteristic elements of Ag, C, and O. As shown in Figure 4c, the barcodes contain metallic silver with binding energies positioned at 375.1 and 369.1 eV. These binding energy values are same with the barcodes obtained by printing only the particle-free silver ink. These results suggest that the incorporation of the taggants does not alter the silver particle formation facilitated by the thermal annealing.

The barcodes fabricated by simultaneous printing of the particle-free silver ink and taggant exhibited high SERS-activity. Figure 5 shows the SERS spectra for three different concentrations of three taggant molecules mixed with the particle-free silver ink. These SERS spectra were obtained following the transfer of the printed patterns on a silicon substrate. The characteristic bands of all taggant molecules could be clearly

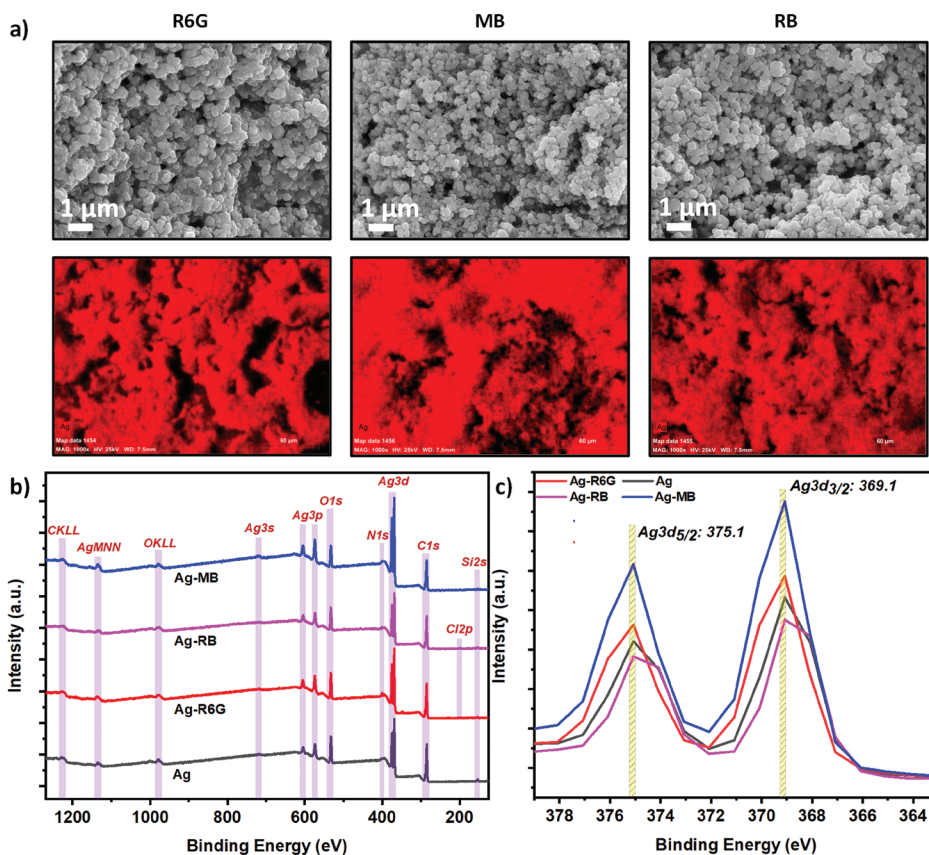


Figure 4. Chemical and structural characterizations of barcodes prepared by co-deposition of taggant molecules and the silver ink. a) SEM images and EDX mapping of silver on the barcodes. b) XPS analysis. c) High-resolution regional XPS spectra of Ag3d.

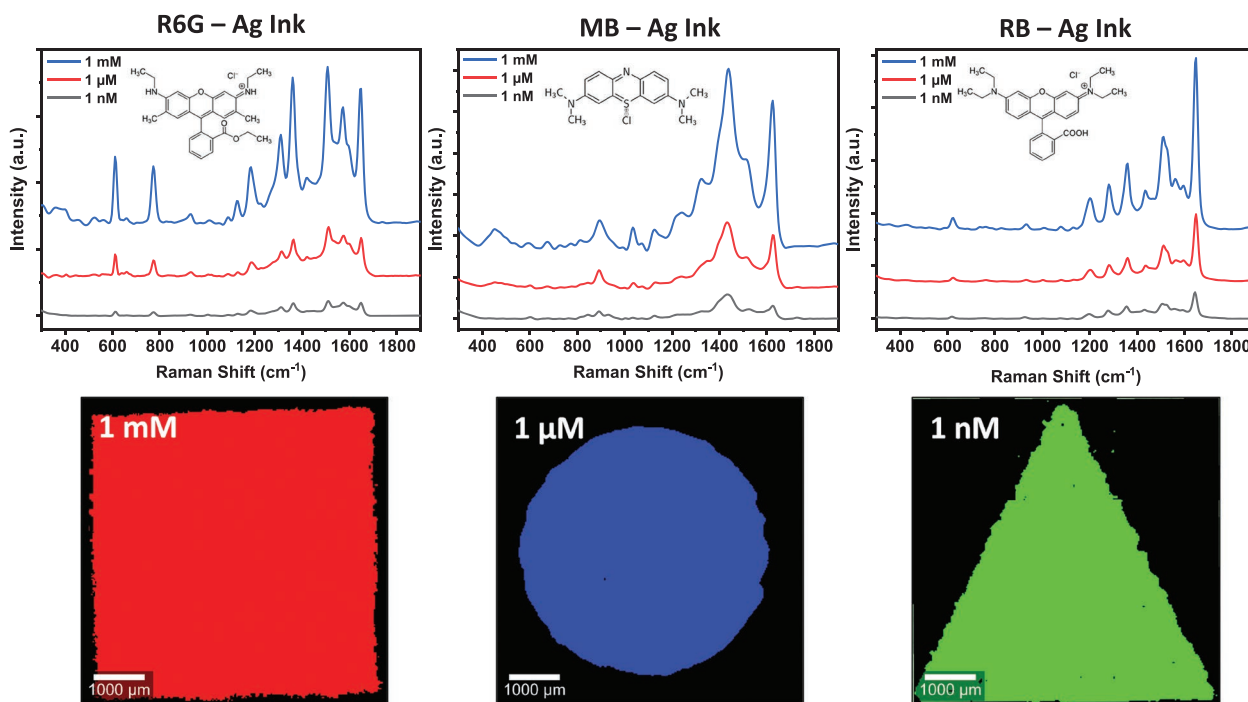


Figure 5. SERS characterization of the SERS barcodes prepared by co-deposition of the silver ink and taggants. The top row refers to SERS spectra for taggants of varied concentrations. The bottom row includes Raman mapping images of the printed features. The mapping image was generated using the Raman shift at positions of 1649 cm⁻¹ for R6G, 1624 cm⁻¹ for MB, and 1280 cm⁻¹ for RB.

distinguished. For RB, these bands are located at 1196 cm^{-1} ($\beta(\text{C-H})$ bend vibration), 1280 cm^{-1} ($\nu(\text{C-C})$ bridge band stretch vibration), and $1359/1648\text{ cm}^{-1}$ (aromatic stretch vibrations).^[59,60] For MB, these bands include 451 cm^{-1} ($\delta(\text{C-N-C})$ skeletal deformation mode), $1392/1432\text{ cm}^{-1}$ ($\nu(\text{C-N})$ symmetric and asymmetric stretches), and 1624 cm^{-1} ($\nu(\text{C-C})$ ring stretches).^[61] These results show that the taggant molecules retain their chemical composition during the processes of mixing with the silver ink, printing, thermal annealing, and transferring. The ability to detect taggant molecules at relatively low (e.g., $1 \times 10^{-9}\text{ M}$) concentrations shows the high SERS activity obtained by co-deposition of the silver ink and taggants. The Raman mapping of the SERS activity reveals homogeneity across the substrate. Furthermore, the simultaneous deposition of the silver ink and taggants results

in barcodes that are visually indifferent from the ones fabricated by just printing the silver ink. This characteristic is important for an advanced anticounterfeiting system, where even the presence of a SERS based security layer will not be obvious to the users and counterfeiters (Figure S11, Supporting Information).

To determine the size of barcodes that can be efficiently and clearly fabricated using an office type ink-jet printer, we printed QR codes in various sizes (edge lengths of 12, 9, 6, and 3 mm). At all sizes, the characteristic vibration bands of the taggant can be clearly detected in the Raman spectrum. QR codes could be read effectively from the Raman mapping images when the edge length of the QR code is equal or greater than 6 mm (Figure 6a). Note that this result was obtained with an office type ink-jet printer and advanced printing systems^[62,63] can

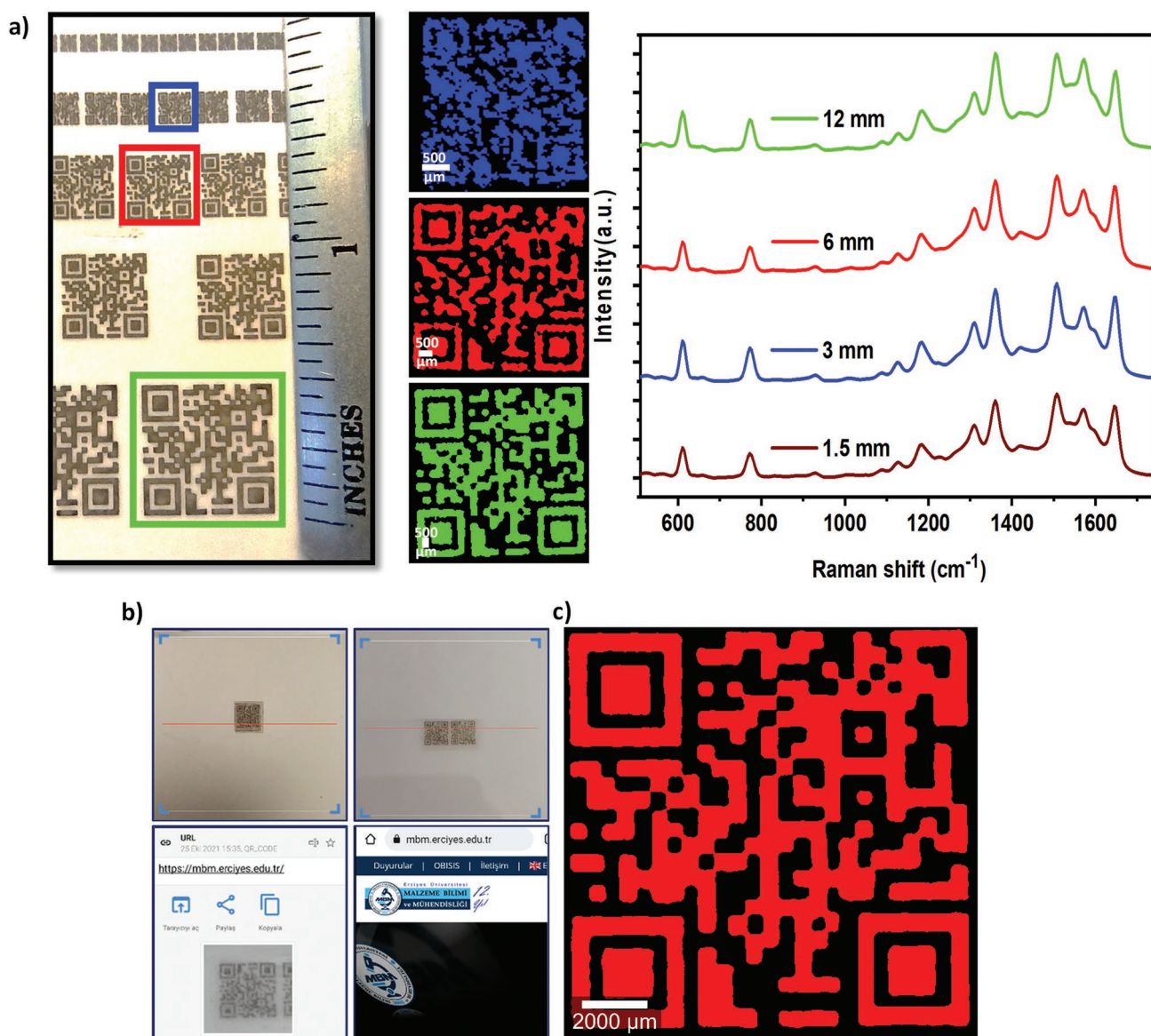


Figure 6. QR Codes. a) QR code of varied sizes. Photograph of printed QR codes and their Raman mapping images. On the right, Raman spectra are given for QR codes of varied edge lengths. Printing was done using a mixture of $1 \times 10^{-3}\text{ M}$ R6G and silver ink. b) Verification of QR codes transferred to two different phones. c) Decoding the Raman security layer of the transferred QR code. The mapping image was generated using the Raman shift at a position of 1649 cm^{-1} .

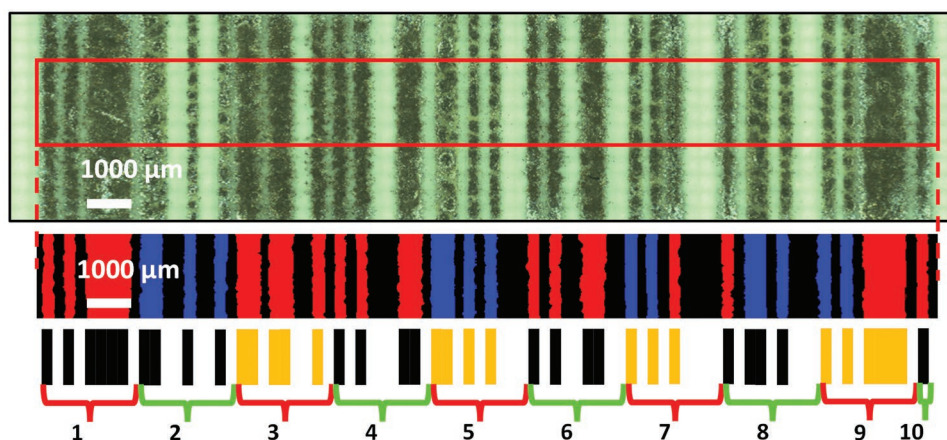


Figure 7. One-dimensional barcode printed with a mixture of taggant molecules (MB and R6G) and silver ink. Optical microscope (top) and Raman mapping (middle) images are presented. The barcode (bottom) encodes the expression of “ERNAM” in the code 93 system.

further reduce the size of barcodes. As a proof of the concept, we transferred the SERS barcodes on the backside of a phone (Figure 6b). The SERS barcode was fabricated using a mixture of the particle-free silver ink and R6G with a concentration of 1×10^{-3} M. Figure 6c presents the Raman mapping image of the barcode transferred to the phone. An advantage of the co-deposition of the silver ink and taggant is the absence of taggant molecules in the background regions. This feature enables a high signal to noise ratio and excellent contrast in Raman mapping images. This Raman mapping image was then scanned using a smart-phone to direct the user to a web-site (Figure S13, Supporting Information). QR code verification process can also be found in Video S1 (Supporting Information).

An inherent advantage of ink-jet printing is the additive deposition of materials without cross-contamination. This capability is important to further augment the complexity of the barcodes and achieve high encoding capacity. To demonstrate this capability, we used linear one-dimensional barcodes. An expression (ERNAM) was then written in linear barcodes according to the Code 93 system. The ink-jet printing was performed on the tattoo paper using mixtures of silver ink and taggant molecules of varying composition. The barcode becomes clearly visible with Raman mapping of the characteristic vibration bands of taggant molecules (Figure 7). In the Raman mapping image, the red and blue bars represent R6G and MB, respectively. The background appears dark, as there are no taggant molecules and plasmonic nanoparticles. In the Code 93 system, each character is represented by three spaces and three bars (see Table S2, Supporting Information, for details). Including start character and termination bar, the “ERNAM” expression consists of 28 bars. Considering that each bar can be printed with two different taggants, the encoding capacity equals to 2^{28} (268435456 combinations).

3. Conclusion

This study has demonstrated the practical fabrication of transferable SERS barcodes using a combination of ink-jet printing and temporary tattoo approach. The key advantage of this

approach is decoupling the barcode preparation process from the final substrate. An important contribution of this study is the use of a particle-free ink formulation previously developed for printed electronics applications for SERS studies. This ink can be printed over large areas in designed patterns without clogging problems that are associated with particle containing compositions. The incorporation of the taggants into the ink and thermal annealing at relatively low temperatures are key for effective fabrication of SERS-active barcodes. In addition to the commonly used active reporter molecules, future studies may employ other Raman-active molecules for encoding. The additive operation of ink-jet printing is important for generating large numbers of SERS barcodes. The substrate independent fabrication, simplicity, minimal usage of materials, and multiplex deposition of taggants offer unprecedented avenues of research in encoding applications.

4. Experimental Section

Materials: Silicon wafers (<100>) were purchased from University Wafer. Silver acetate (99.0%), formic acid ($\geq 95\%$), rhodamine 6G (R6G, 99%), methylene blue (MB, 97%), and rhodamine B (RB, $\geq 95\%$) were purchased from Sigma–Aldrich. Ethanol (96%) and ammonia solution (25%) were purchased from Merck. HP Deskjet Ink Advantage 2060 office-type printer was used for ink-jet printing. Temporary tattoo (Yuanteng) paper was used as an aqueous transfer paper. This temporary tattoo paper was referred to as the tattoo paper throughout the manuscript.

Preparation of Particle-Free Reactive Silver Inks: Particle-free reactive silver ink was prepared by following the previously reported approach.^[64] Silver acetate (0.5 g) was dissolved in 1.25 mL of ammonia solution and then mixed at 575 rpm using a magnetic stirrer at room temperature. After observing that the silver acetate was completely dissolved, 0.1 mL formic acid was slowly added while the solution was continued to mix. With the addition of formic acid, silver nanoparticles formed and the solution continued to be mixed for 5 min. The solution was centrifuged at 4000 rpm for 30 min to settle down and remove silver nanoparticles. The supernatant was taken and used as ink to fabricate SERS-active barcodes.

Fabrication of SERS Barcodes Using Inkjet Printing: Before printing, the cartridge was emptied, thoroughly cleaned by repeatedly washing in ethanol under sonication and dried with air. The particle-free reactive silver ink or taggant molecule-ink mixture was filled in an empty

cartridge. User designed patterns were then printed in the high-quality mode (600 dpi) on the tattoo paper. Silver-printed tattoo papers were annealed at 135 °C for 2 min to form silver nanoparticles.

Transfer of SERS Barcodes: The transfer of the SERS barcodes was performed by placing the sticky paper on top of the printed tattoo paper. The barcodes were then transferred to the object of interest by sticking the tattoo paper with a gentle application of pressure. The transfer process was completed by rubbing with a damp cloth on paper.

Characterization: Morphology and chemical composition of SERS barcodes were studied using scanning electron microscopy (SEM, Zeiss EVO LS10) and energy-dispersive X-ray spectroscopy (EDX, Bruker) at 25 keV. The surface compositions of barcodes were studied with X-ray photoelectron spectroscopy (XPS, Specs-Flex) using an XRM50 (UXC1000) source of exciting radiation (1486.71 eV). Thin film X-ray diffraction (XRD) data were recorded using the Panalytical Empyrean diffractometer operating at 40 kV and 30 mA by using Cu K α radiation source.

SERS Measurements: SERS measurements were acquired using a confocal Raman microscope (Alpha 300 M+, WITec, Germany) equipped with a 532 nm wavelength as an excitation source. The laser beam with an effective power of 3.2 mW was focused on the surface through a 100 \times microscope objective. All spectra were collected by Raman mapping using an integration time of 0.1 s and step size of 1 μ m. The large area Raman mapping images (butterfly and barcodes) were generated with a step size of 20 μ m. Patterned silver ink structures were identified by k-means cluster analysis (WITec Project Plus software 5.1). A baseline correction was performed for each spectrum.

The AEF of the SERS barcodes was calculated using the following Equation:^[65]

$$AEF = \frac{I_{SERS}/C_{SERS}}{I_{Raman}/C_{Raman}} \quad (1)$$

where I_{SERS} and I_{Raman} are the peak intensity at 1649 cm^{-1} obtained from SERS barcodes and Si wafer, respectively. C_{SERS} and C_{Raman} are the concentration of R6G used for SERS barcode and Si wafer, respectively.

Three different taggants (R6G, MB, RB) were used for taggant ink mixture prints. A 1×10^{-3} M taggant-silver ink stock was prepared by mixing 10×10^{-3} M taggants with silver ink at a 1:9 ratio. The 1×10^{-6} and 1×10^{-9} M taggant-silver ink mixtures were obtained from 1mM concentration.

Statistical Analysis: To probe the sample to sample variability, SERS intensities from ten different samples were measured using R6G with a concentration of 100×10^{-6} M. The results are presented in Table S1 (Supporting Information) with a mean value and standard deviation for different Raman vibrations.

Supporting Information

Supporting Information is available from the Wiley Online Library or from the author.

Acknowledgements

This work was supported by the Research Fund of the Erciyes University (Project Number FKB-2020-9717). F.S. and Z.G. were supported by the Council of Higher Education of Turkey (100/2000 YÖK Doctoral Scholarship).

Conflict of Interest

The authors declare no conflict of interest.

Data Availability Statement

The data that support the findings of this study are available from the corresponding author upon reasonable request.

Keywords

anti-counterfeiting, ink-jet printing, SERS barcodes, temporary tattoo

Received: January 9, 2022

Revised: February 4, 2022

Published online: March 28, 2022

- [1] Organisation for Economic Co-operation, and Development, *European Union. Intellectual Property Office.*, OECD-iLibrary – York University, **2019**, 60.
- [2] T. Mavlanova, R. Benbunan-Fich, <http://doi.org/10.2753/JEC1086-4415150203> **2014**, 15, 79.
- [3] B. Farrand, <https://doi.org/10.1080/23745118.2018.1430721> **2018**, 19, 338.
- [4] H. Zhang, D. Hua, C. Huang, S. K. Samal, R. Xiong, F. Sauvage, K. Braeckmans, K. Remaut, S. C. De Smedt, *Adv. Mater.* **2020**, 32, 1905486.
- [5] R. J. Ziance, *J. Am. Pharm. Assoc.* **2008**, 48, e71.
- [6] T. Burki, *Lancet Infect. Dis.* **2010**, 10, 585.
- [7] E. L. Prime, D. H. Solomon, *Angew. Chem., Int. Ed.* **2010**, 49, 3726.
- [8] J. Jiang, J. Chen, *Sustainability* **2021**, 13, 6016.
- [9] N. Kayaci, R. Ozdemir, M. Kalay, N. B. Kiremitler, H. Usta, M. S. Onses, *Adv. Funct. Mater.* **2021**, 2108675.
- [10] F. Kaboli, N. Ghazyani, M. Riahi, H. Zare-Behtash, M. H. Majles Ara, E. Heydari, *ACS Appl. Nano Mater* **2019**, 2, 3590.
- [11] M. Wang, B. Duong, H. Fenniri, M. Su, *Nanoscale* **2015**, 7, 11240.
- [12] B. Yoon, J. Lee, I. S. Park, S. Jeon, J. Lee, J.-M. Kim, *J. Mater. Chem. C* **2013**, 1, 2388.
- [13] H. Tan, G. Gong, S. Xie, Y. Song, C. Zhang, N. Li, D. Zhang, L. Xu, J. Xu, J. Zheng, *Langmuir* **2019**, 35, 11503.
- [14] Y. Qin, Y. Bai, P. Huang, F. Y. Wu, *ACS Appl. Nano Mater.* **2021**, https://doi.org/10.1021/ACSANM.1C02148/SUPPL_FILE/AN1C02148_SI_001.PDF.
- [15] H. Hu, H. Zhong, C. Chen, Q. Chen, *J. Mater. Chem. C* **2014**, 2, 3695.
- [16] B. Song, H. Wang, Y. Zhong, B. Chu, Y. Su, Y. He, *Nanoscale* **2018**, 10, 1617.
- [17] R. Li, Y. Zhang, J. Tan, J. Wan, J. Guo, C. Wang, *ACS Appl. Mater. Interfaces* **2016**, 8, 9384.
- [18] Y. Cui, R. S. Hegde, I. Y. Phang, H. K. Lee, X. Y. Ling, *Nanoscale* **2013**, 6, 282.
- [19] N. Torun, I. Torun, M. Sakir, M. Kalay, M. S. Onses, *ACS Appl. Mater. Interfaces* **2021**, 13, 11247.
- [20] * K. Kneipp, H. Kneipp, I. Itzkan, R. R. Dasari, M. S. Feld, *Chem. Rev.* **1999**, 99, 2957.
- [21] D. L. Jeanmaire, R. P. Van Duyne, *J. Electroanal. Chem.* **1977**, 84, 1.
- [22] M. Sakir, S. Pekdemir, A. Karatay, B. Küçüköz, H. H. Ipekci, A. Elmali, G. Demirel, M. S. Onses, *ACS Appl. Mater. Interfaces* **2017**, 9, 39795.
- [23] H. N. Huang, S. Y. Wang, W. H. Chiang, *ACS Appl. Nano Mater.* **2021**, 4, 10360.
- [24] S. Karagoz, N. B. Kiremitler, M. Sakir, S. Salem, M. S. Onses, E. Sahmetioglu, A. Ceylan, E. Yilmaz, *Ecotoxicol. Environ. Saf.* **2020**, 188, 109856.
- [25] X. S. Zheng, I. J. Jahn, K. Weber, D. Cialla-May, J. Popp, *Spectrochim. Acta Part A Mol. Biomol. Spectrosc.* **2018**, 197, 56.
- [26] M. M. Joseph, N. Narayanan, J. B. Nair, V. Karunakaran, A. N. Ramya, P. T. Sujai, G. Saranya, J. S. Arya, V. M. Vijayan, K. K. Maiti, *Biomaterials* **2018**, 181, 140.
- [27] S. Srivastav, A. Dankov, M. Adanalic, R. Grzeschik, V. Tran, S. Pagel-Wieder, F. Gessler, I. Spreitzer, T. Scholz, B. Schnierle, O. E. Anastasiou, U. Dittmer, S. Schlucker, *Anal. Chem.* **2021**, 93, 12391.

- [28] M. Sajitha, B. Abraham, R. B. Nelliyil, K. Yoosaf, *ACS Appl. Nano Mater.* **2021**, *4*, 10038.
- [29] D. Cialla-May, X. S. Zheng, K. Weber, J. Popp, *Chem. Soc. Rev.* **2017**, *46*, 3945.
- [30] Y. Liu, Y. H. Lee, Q. Zhang, Y. Cui, X. Y. Ling, *J. Mater. Chem. C* **2016**, *4*, 4312.
- [31] K. J. Si, D. Sikdar, L. W. Yap, J. K. K. Foo, P. Guo, Q. Shi, M. Premaratne, W. Cheng, *Adv. Opt. Mater.* **2015**, *3*, 1710.
- [32] X. Liu, J. Wang, L. Tang, L. Xie, Y. Ying, *Adv. Funct. Mater.* **2016**, *26*, 5515.
- [33] Y. Liu, Y. H. Lee, M. R. Lee, Y. Yang, X. Y. Ling, *ACS Photonics* **2017**, *4*, 2529.
- [34] Y. Gu, C. He, Y. Zhang, L. Lin, B. D. Thackray, J. Ye, *Nat. Commun.* **2020**, *11*, 516.
- [35] H. Cheng, Y. Lu, D. Zhu, L. Rosa, F. Han, M. Ma, W. Su, P. S. Francis, Y. Zheng, *Nanoscale* **2020**, *12*, 9471.
- [36] Y. Zhou, G. Zhao, J. Bian, X. Tian, X. Cheng, H. Wang, H. Chen, *ACS Appl. Mater. Interfaces* **2020**, *12*, 28532.
- [37] Q. Li, F. Chen, J. Kang, J. Su, F. Huang, P. Wang, X. Yang, Y. Hou, *Adv. Funct. Mater.* **2021**, *31*, 2010537.
- [38] S. Liu, X. Tian, J. Guo, X. Kong, L. Xu, Q. Yu, A. X. Wang, *Appl. Surf. Sci.* **2021**, *567*, 150861.
- [39] Y. Huo, S. Curry, A. Trowbridge, X. Xu, C. Jiang, *Mater. Adv.* **2021**, *2*, 5116.
- [40] Y. Feng, Y. Gu, M. Wang, X. Xu, Y. Liu, D. Li, *Adv. Mater. Interfaces* **2021**, *8*, 2002246.
- [41] C. L. Lay, C. S. L. Koh, J. Wang, Y. H. Lee, R. Jiang, Y. Yang, Z. Yang, I. Y. Phang, X. Y. Ling, *Nanoscale* **2018**, *10*, 575.
- [42] A. F. Smith, S. E. Skrabalak, *J. Mater. Chem. C* **2017**, *5*, 3207.
- [43] Y. Cui, I. Y. Phang, Y. H. Lee, M. R. Lee, Q. Zhang, X. Y. Ling, *Chem. Commun.* **2015**, *51*, 5363.
- [44] D. Li, L. Tang, J. Wang, X. Liu, Y. Ying, *Adv. Opt. Mater.* **2016**, *4*, 1475.
- [45] S. Pekdemir, H. H. Ipekci, M. Serhatlioglu, C. Elbuken, M. S. Onses, *J. Colloid Interface Sci.* **2021**, *584*, 11.
- [46] K. E. Relyea, St. Joseph, Wis., *Printed, Removable Body Tattoos on a Translucent Substrate*, **1986**, 4,594,276.
- [47] G. E. Bonacchini, C. Bossio, F. Greco, V. Mattoli, Y. H. Kim, G. Lanzani, M. Caironi, *Adv. Mater.* **2018**, *30*, 1706091.
- [48] Y. Zheng, W. Panatdasirisuk, J. Liu, A. Tong, Y. Xiang, S. Yang, *Adv. Mater. Technol.* **2020**, *5*, 2000564.
- [49] Q. Yan, X. Xie, Y. Liu, S. Wang, M. Zhang, Y. Chen, Y. Si, *J. Hazard. Mater.* **2019**, *371*, 304.
- [50] W. B. Zhao, J. J. Zhu, H. Y. Chen, *J. Cryst. Growth* **2003**, *258*, 176.
- [51] E. Kirubha, P. K. Palanisamy, *Adv. Nat. Sci. Nanosci. Nanotechnol.* **2014**, *5*, 045006.
- [52] M. Sakir, E. Yilmaz, M. S. Onses, *Microchem. J.* **2020**, *154*, 104628.
- [53] I. Korkmaz, M. Sakir, G. Sarp, S. Salem, I. Torun, D. Volodkin, E. Yavuz, M. S. Onses, E. Yilmaz, *J. Mol. Struct.* **2021**, *1223*, 129258.
- [54] J. Lin, Y. Shang, X. Li, J. Yu, X. Wang, L. Guo, *Adv. Mater.* **2017**, *29*, 1604797.
- [55] Y. Xie, Y. Jin, Y. Zhou, Y. Wang, *Appl. Surf. Sci.* **2014**, *313*, 549.
- [56] I. E. Pavel, K. S. Alnajjar, J. L. Monahan, A. Stahler, N. E. Hunter, K. M. Weaver, J. D. Baker, A. J. Meyerhoefer, D. A. Dolson, *J. Chem. Educ.* **2011**, *89*, 286.
- [57] W. W. Yu, I. M. White, *Anal. Chem.* **2010**, *82*, 9626.
- [58] C. M. Wang, P. K. Roy, B. K. Juluri, S. Chattopadhyay, *Sensors Actuators B Chem* **2018**, *261*, 218.
- [59] C. Fang, A. Agarwal, K. D. Buddharaju, N. M. Khalid, S. M. Salim, E. Widjaja, M. V. Garland, N. Balasubramanian, D. L. Kwong, *Biosens. Bioelectron.* **2008**, *24*, 216.
- [60] F. Sahin, N. Celik, A. Ceylan, S. Pekdemir, M. Ruzi, M. Serdar Onses, *Chem. Eng. J.* **2021**, 133445.
- [61] G. N. Xiao, S. Q. Man, *Chem. Phys. Lett.* **2007**, *447*, 305.
- [62] M. S. Onses, E. Sutanto, P. M. Ferreira, A. G. Alleyne, J. A. Rogers, *Small* **2015**, *11*, 4237.
- [63] S. Yakunin, J. Chaaban, B. M. Benin, I. Cherniukh, C. Bernasconi, A. Landuyt, Y. Shynkarenko, S. Bolat, C. Hofer, Y. E. Romanyuk, S. Cattaneo, S. I. Pokutnyi, R. D. Schaller, M. I. Bodnarchuk, D. Poulidakos, M. V. Kovalenko, *Nat. Commun.* **2021**, *12*, 981.
- [64] S. B. Walker, J. A. Lewis, *J. Am. Chem. Soc.* **2012**, *134*, 1419.
- [65] S. Pekdemir, I. Torun, M. Sakir, M. Ruzi, J. A. Rogers, M. S. Onses, *ACS Nano* **2020**, *14*, 8276.